This article has been accepted for publication in a future issue of this journal, but has not been fully edited. Content may change prior to final publication. Citation information: DOI 10.1109/TSG.2017.2729592, IEEE Transactions on Smart Grid



# Incorporating Wind Energy in Power System Restoration Planning

Amir Golshani, *Student Member, IEEE,* Wei Sun, *Member, IEEE,* Qun Zhou, *Member, IEEE,* Qipeng P. Zheng, *Member, IEEE,* and Yunhe Hou, *Senior Member, IEEE*

***Abstract*—Wind energy is rapidly growing. While wind brings us clean and inexpensive energy, its inherent variability and uncertainty present challenges for the power grid. In particular, employing wind energy for power system restoration is very challenging. A fast and reliable restoration plays a vital role to achieve the self-healing power grid. This paper develops a novel offline restoration planning tool for harnessing wind energy to enhance grid resilience. The Wind-for-Restoration problem is formulated as a stochastic mixed-integer linear programming problem with generated wind energy scenarios. The problem is then decomposed into two stages and solved with the integer L-shaped algorithm. Numerical experiments have been conducted through different case studies using the modified IEEE 57-bus system. The developed tool can provide the scheduled wind power at each restoration time. The impact of wind energy is investigated from the aspects of location and inertia capability, as well as wind penetration, fluctuation, and uncertainty. Moreover, a dynamic response validation tool is developed to validate the results of optimization problem in a dynamic simulation software. Simulation results demonstrate that the optimal wind harnessing strategy can help improve system restoration process and enhance system resilience.**

***Index Terms*—Integer L-shaped algorithm, mixed-integer linear programming, power system restoration, stochastic optimization, wind uncertainty.**

## NOMENCLATURE

Decision variables:

| | |
|---|---|
| $u_{g,t}^{\text{on}}$ | Binary variable equal to 1 if unit $g$ is on at time $t$. |
| $u_{g,t}^{\text{start}}$ | Binary variable equal to 1 if unit $g$ is in start-up period at time $t$. |
| $u_{w,t}$ | Binary variable equal to 1 if wind farm $w$ is on at time $t$. |
| $t_g^{\text{start}}$ | Start-up time of unit $g$. |
| $P_{g,t}$ | Scheduled power of unit $g$ at time $t$ after connecting to the grid. |
| $P_{g,t}^{\text{start}}$ | Start-up power of unit $g$ at time $t$. |
| $u_{n(m),t}$ | Binary variable equal to 0/1 if bus $n/m$ is de-energized/energized at time $t$. |
| $u_{l,t}$ | Binary variable equal to 0/1 if the line $l$ is de-energized/energized at time $t$. |
| $P_{d,t}, Q_{d,t}$ | Amount of real and reactive loads restored at load bus $d$ and time $t$. |
| $P_{w,t}, Q_{w,t}$ | Wind farm scheduled active and reactive power at time $t$. |
| $P_{l,t}^{\text{flow}}, Q_{l,t}^{\text{flow}}$ | Real and reactive power flows in line $l$ at time $t$. |
| $\Delta P_t^{\max}$ | Total load pickup capability at time $t$. |
| $R_t, R_{g,t}$ | Total dynamic reserve and dynamic reserve share of unit $g$ at time $t$. |
| $R_{d,t}$ | Load shedding share of load bus $d$ in dynamic reserve at time $t$. |
| $R_{w,t}$ | Dynamic reserve share of wind farm $w$ at time $t$. |
| $V_{n,t}, \theta_{n,t}$ | Voltage magnitude and angle of bus $n$ at time $t$. |
| $y_{nm,t}$ | Piecewise linear approximation of $\cos(\theta_n - \theta_m)$ at time $t$. |
| $Q(x), \phi$ | Second-stage objective function and estimated second-stage objective function. |

Constant parameters:

| | |
|---|---|
| $P_g^{\max}, P_g^{\min}$ | Maximum and minimum real power capacities of unit $g$. |
| $Q_g^{\max}, Q_g^{\min}$ | Maximum and minimum reactive power capacities of unit $g$. |
| $P_g^{\text{start}}$ | Cranking power of unit $g$. |
| $\alpha_d$ | Priority factor of load $d$. |
| $P_d^{\max}, Q_d^{\max}$ | Maximum restorable active and reactive loads at load bus $d$. |
| $T_g^{\text{start}}$ | Start-up duration of unit $g$. |
| $H_g, H_w, H_t^{\text{eq}}$ | Inertia of unit $g$, wind farm $w$, and total inertia of all online generation units. |
| $RR_g$ | Ramping rate of generation unit $g$. |
| $f^{\min}, f^{\text{db}}, f^0$ | Minimum allowable frequency (Hz), governor's dead band (mHz), and nominal frequency (Hz). |
| $\pi_s$ | Probability of scenario $s$. |
| $V^{\min}, V^{\max}$ | Minimum and maximum limits of bus voltage. |
| $\beta_z, \beta_I, \beta_p$ | Coefficients of constant impedance, constant current and constant power loads. |
| $g_{nm}, b_{nm}, b_{nm}^c$ | Conductance, susceptance, and shunt susceptance of the transmission line between buses $n$ and $m$. |
| $K$ | Number of segments in cosine function |

This work is supported in part by the U.S. National Science Foundation under Grant ECCS-1552073 and Grant CMMI-1355939, and AFRL Mathematical Modeling and Optimization Institute.

A. Golshani, W. Sun, and Q. Zhou are with the Department of Electrical and Computer Engineering, and Q. P. Zheng is with the Department of Industrial Engineering and Management Systems, University of Central Florida, Orlando, FL. 30816 USA (e-mail: amir.golshani@knights.ucf.edu, sun@ucf.edu, qun.zhou@ucf.edu, and qipeng.zheng@ucf.edu).

Y. Hou is with the Electrical and Electronic Engineering Department, the University of Hong Kong, Pokfulam, Hong Kong, (e-mails: yhhou@eee.hku.hk).

This article has been accepted for publication in a future issue of this journal, but has not been fully edited. Content may change prior to final publication. Citation information: DOI 10.1109/TSG.2017.2729592, IEEE Transactions on Smart Grid



approximation.

Sets:

| | |
|---|---|
| $T$, $S$ | Sets of restoration times and scenarios. |
| $D$, $D_{\text{UFLS}}$ | Sets of loads and loads with under-frequency load shedding relays. |
| $G$, $B$, $L$, $W$ | Sets of generation units, buses, transmission lines, and wind farms. |
| $G_{\text{NBSU}}$, $G_{\text{BSU}}$ | Sets of non-black-start and black-start generation units. |

Indices:

| | |
|---|---|
| $n, m$ | Indices for buses at both ends of the lines. |
| $l$ | Index for lines. |
| $b_g$, $b_d$, $b_w$ | Indices for generators, loads and wind farms buses. |
| $g$, $d$, $t$, $w$, $s$ | Indices for generators, loads, time periods, wind farms, and scenarios. |

## I. Introduction

WIND power generation has been rapidly increasing over the last decade. The U.S. Department of Energy released an update for its earlier report, entitled 20% wind energy by 2030, showing that the wind power's installed capacity has exceeded the level envisioned in 2008 [1]. Wind power has been actively incorporated in power system operations under *normal* operating conditions, such as unit commitment and economic dispatch [2], [3]. It brings tremendous environmental, social, and economic benefits. Nevertheless, due to its inherent variability and uncertainty, wind power is rarely used in *emergency* conditions such as power system restoration.

Large-scale power outages become more common place with the growth in frequency and strength of natural disasters and cyber-attacks, which poses a direct threat to our energy infrastructure. Essential to achieving the self-healing power grid is a fast and reliable restoration procedure for system operators to re-start generating units, establish a transmission network, pick up customer loads, and eventually restore the system to its normal condition [4].

As the U.S. power grid undergoes massive transition to the smart grid era, increased reliance on renewable energy could adversely impact power grid resilience and system restoration. While renewable bring us clean and inexpensive energy, their inherent variability and uncertainty present new challenges. Power grids may be jeopardized owing to the different characteristics and unexpected operations of renewable sources. For instance, one of the causes for South Australia blackout of 2016 was the shutdown of wind turbines due to the high wind speed and voltage ride-through protection mechanism [5].

Most independent system operators (ISOs) are conservative on employing wind power for system restoration. For instance, Independent Electricity System Operator (IESO) excludes wind energy resources from the restoration process and keep them out of service until the latter stages of restoration [6]. Australian Energy Market Operator (AEMO) does not utilize wind farms in the initial stages of restoration because of their variable nature or unavailability of transmission capacity [5]. However, with the increasing penetration levels and availability of wind turbines, exclusion of wind power will prolong the recovery time and leave the vast majority of loads unserved. Thus, a new restoration paradigm with contribution from wind power is urgently needed.

Research on utilizing large-scale renewable energy sources for power system restoration is limited to date. Reference [7] discussed several aspects of power system restoration considering wind farm participation. It proposed a supplementary control on doubly fed induction generators (DFIGs) to reduce the negative effect of wind power on system restoration. Reference [8] discussed DFIG wind generators participating as black start resources. The integration of energy storage in the DC link of DFIGs is proposed to ensure a smooth load pickup process. In [9], a power system restoration strategy using utility-scale wind parks with HVDC connection is presented. Wind parks can participate in primary frequency control at the initial restoration phase to improve system stability. An optimal restoration time of renewable energy sources is discussed in [10]. The results show that inclusion of renewable energy sources can help reduce the unserved energy.

Most of the aforementioned studies focused on the control aspects of wind generators, and the control strategies were implemented based on a pre-defined restoration plan. Thus, the most challenging problem of wind variability and uncertainty during the restoration period remained unsolved. In this paper, we address these challenges and propose an offline restoration planning tool. This tool can be utilized by transmission system operators (TSOs) in the planning phase of restoration to effectively and securely harness wind energy. The tool can also be adopted in system operator trainings and drills at control centers, which enables operators to study the impact of wind farm location, penetration level, inertial response, and fluctuations on the restoration process. In addition, a dynamic response validation tool is developed to validate the results from this offline restoration planning tool. Python scripts are developed to automatically generate case studies for each restoration step and exploit functionalities of the commercial time-domain simulation tool, e.g. Power System Simulator for Engineering (PSS/E).

The remainder of this paper is organized as follows. Section II introduces the proposed optimization tool. Section III presents system restoration problem with the MILP formulation considering wind power participation. Section IV extends the deterministic formulation to a stochastic optimization with a set of wind power scenarios. Section V presents the solution methodology using a two stage decomposition and the integer L-shaped algorithm. In section VI, the proposed model is applied to the IEEE 57-bus system test case. Conclusion marks are provided in section VII.

## II. The Proposed Off-line Restoration Tool

After a widespread power outage or blackout, power system operators work diligently to bring the system back to its normal state. System restoration consists of the following tasks: preparation and planning, black-start units (BSUs) start-up, transmission lines energization, non-black-start units (NBSUs) start-up, and load pickup [11], [12].

Wind energy resources can be considered as a third type of generating units. Like BSUs, wind generators can supply

This article has been accepted for publication in a future issue of this journal, but has not been fully edited. Content may change prior to final publication. Citation information: DOI 10.1109/TSG.2017.2729592, IEEE Transactions on Smart Grid



cranking power to other generators. Like NBSUs, wind generators can provide reactive power to energize transmission lines and restore critical loads. Wind generators can also contribute to system frequency control. On the other hand, wind generators differ from conventional BSUs and NBSUs in the following aspects: 1) they are intermittent and weather-dependent in nature; 2) their power can be highly fluctuate and cause large ramping events; and 3) they may reduce system inertia (without supplementary control). Additionally, they have high ramping rate and can be started fast. With these characteristics, harnessing wind power in system restoration needs a thorough investigation and formulation.

As power sectors have undergone restructuring in recent years, the impacts of restructuring efforts on power system restoration should be taken into account. In fact, independent entities aim at maximizing their own profits while exchanging information during the restoration process. Following a blackout, the affected TSOs control and coordinate the operation of generating sources, transmission facilities, and loads within their footprints [13]. For instance, each TSO coordinates with generator operators (GOs) to reconnect tripped generators, and with distribution system operators (DSOs) to reconnect loads. After obtaining the required data from GOs and DSOs, TSO provides restoration plans based on the current system status. Once the TSO submits its restoration plan, GOs and DSOs should comply with the instructions.

The proposed restoration tool is depicted in Fig. 1. Initially, TSO identifies the amount of affected generators and loads. GOs provide TSO with the information of maximum power generation capabilities, cranking powers of available generation units and their ramping capabilities. Assuming wind generators are operated like NBSUs, wind turbine operators (WTOs) send the forecasted wind power to TSO. TSO also needs to identify the amount and location of loads from DSOs. Based on these input data and initial assessment, a number of constraints including generator start-up, line/bus energization, load pickup, dynamic reserve, and wind generator characteristic can be constructed and incorporated into the optimization tool. With perfect wind forecast data, Fig.1 represents a deterministic optimization problem. However, expecting perfect forecast is unrealistic in practice, and in order to cope with its intrinsic error, the deterministic formulation is extended to a stochastic optimization.

In the stochastic optimization problem, the first-stage decisions are obtained from the master problem prior to the uncertainty unfold. From Fig. 1, one can observe that GOs provide TSO with the start-up data and characteristics of BSU and NBSUs. Additionally, TSO receives the status of transmission lines/buses including their initial conditions and availability times for restoration period. WTOs send wind farms forecast data including their maximum generation capabilities. These data are required for solving the master problem. The second-stage decisions are scenario dependent and obtained from the subproblems. The scenarios are generated from forecasted wind power data representing the real-world uncertainties. GOs, DSOs, and WTOs also provide TSO with various data that should be included in the second-stage problem. Generators' ramping capabilities, governors' characteristics, amount

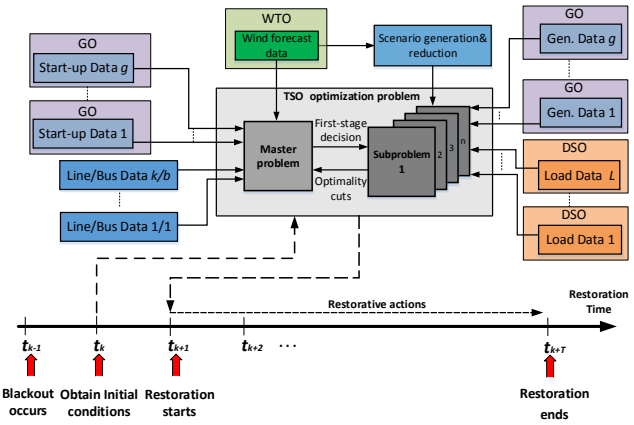


Fig. 1. Off-line optimization tool adopted by TSO to harness wind energy.

and locations of loads, wind power forecast data and its error are some of the required data for solving the subproblems corresponding to each scenario.

A solution methodology of two-stage decomposition is proposed for the stochastic MILP problem. Then, an optimality cut is generated and fed back to the first-stage problem and re-solve the updated master problem. This iterative process continues until the convergence criteria are met. TSO solves this two-stage stochastic MILP problem, and provides the restoration plan to GOs, WTOs, and DSOs, who will be responsible for carrying out restoration actions. For example, GOs are notified of the start-up and synchronization times of generators and implement the generator startup; WTOs operate wind generators based on the provided connection times and the scheduled wind power output; DSOs receive the load pickup values and implement the load pickup actions.

## III. Problem Formulation

Power system restoration is a complex combinatorial optimization problem. The objective is to maximize the total generation capability and minimize the unserved load during the entire restoration period, denoted by

$$\max\Bigg(\sum_{t\in T}\sum_{g\in G}(P_g^{\max}-P_g^{\text{start}})u_{g,t}^{\text{on}}+\sum_{t\in T}\sum_{w\in W}\bar{P}_{w,t}u_{w,t} -\sum_{t\in T}\sum_{d\in D}\alpha_d(P_d^{\max}-P_{d,t})\Bigg) \tag{1}$$

where binary variable $u_{g,t}^{\text{on}}$ denotes the status of generating unit $g$ at restoration time $t$, parameters $P_g^{\max}$ and $P_g^{\text{start}}$ represent the generation capacity and required cranking power of unit $g$. $\alpha_d$ is the load priority factor, $P_d^{\max}$ is the maximum restorable load, and $P_{d,t}$ denotes the total restored load at restoration time $t$. Note that wind farm $w$ *directly* contribute to the total generation capability with the term of $\bar{P}_{w,t}u_{w,t}$, where $\bar{P}_{w,t}$ is wind farm forecasted power and $u_{w,t}$ is the status.

Multiple constraints need to be considered for restoration, including generator start-up functions, energization constraints, power balance constraints, load characteristics and load pickup constraints, and dynamic reserve constraints. All decision variables satisfy $\forall t \in T$, $\forall g \in G$, $\forall d \in D$, $\forall (n, m, b_w, b_d, b_g) \in B$, $\forall l \in L$, $w \in W$.

This article has been accepted for publication in a future issue of this journal, but has not been fully edited. Content may change prior to final publication. Citation information: DOI 10.1109/TSG.2017.2729592, IEEE Transactions on Smart Grid



*a) Initial Conditions:* After a blackout and before running the optimization tool, TSO calls for obtaining the initial conditions of power network to identify the current status of power grid. On one hand, natural disasters may cause widespread destruction in the major power grid infrastructure. Thus, some grid components may not be available for restoration right after the blackout. On the other hand, some incidents such as cyber-attacks are intended to target substations, power plants, or local utilities which may cause the partial blackouts. In such cases, major parts of network are not affected and do not require any restoration actions.

In this paper we assume that a total blackout case occurs without bringing damages to system components as well as the major infrastructure. Conventional generation units as well as wind turbines are readily available to contribute to the restoration. However, one can simply modify these constraints for any given initial conditions. Constraints (2) and (3) imply that at $t = 0$, all NBSUs are off and transmission lines/buses are de-energized. Constraint (4) shows that the restoration process is commenced at $t = 1$ by starting the BSU.

$$u^{\text{start}}_{g,t=0} = 0 \quad \forall g \in G_{\text{NBSU}} \tag{2}$$

$$u_{l,t=0} = 0 \quad u_{n,t=0} = 0 \tag{3}$$

$$u^{\text{start}}_{g,t=1} = 1 \quad \forall g \in G_{\text{BSU}} \tag{4}$$

*b) Generator Start-up Functions:* The start-up characteristic of NBSUs is shown in (5), where integer variable $t^{\text{start}}_g$ and parameter $T^{\text{start}}_g$ represent start-up and cranking times. $P^{\text{start}}_g$ is the cranking power of generator $g$. To integrate each generator's start-up function into the first-stage problem, constraint (5) should be converted into MILP form. Our previous work has presented the similar generator start-up curve together with a method which adopts new binary and linear decision variables to define generator start-up function in linear form [14].

$$P^{\text{start}}_{g,t} = \begin{cases} 0 & 0 < t < t^{\text{start}}_g \\ P^{\text{start}}_g & t^{\text{start}}_g \le t \le t^{\text{start}}_g + T^{\text{start}}_g \end{cases} \tag{5}$$

Note that for $t \le (t^{\text{start}}_g + T^{\text{start}}_g)$ generators' output power follow their start-up function, $P^{\text{start}}_{g,t}$. Whereas, for $t > (t^{\text{start}}_g + T^{\text{start}}_g)$, generators' scheduled power are determined in constraints (11) and (14), denoted by $P_{g,t}$.

*c) Energization Constraints:* Units need to be started; buses and lines need to be energized. Constraint (6) shows that each NBSU's start-up sequence is initiated only after energization of its respective bus, $b_g$. Binary variable $u^{\text{on}}_{g,t}$ can be derived from (7). Wind generator $w$ cannot be started until its bus $b_w$ is energized in (8). Assuming that a transmission line $l$ connects buses $n$ and $m$, if both buses are de-energized at restoration time $t$, then the transmission line $l$ is de-energized at time $t$ in (9). In (10), a transmission line $l$ can be energized one restoration time unit after energization of one of its connected buses.

$$u^{\text{start}}_{g,t} \le u_{b_g,t} \tag{6}$$

$$\sum_{t\in T}(1 - u^{\text{on}}_{g,t}) \ge \sum_{t\in T}(1 - u^{\text{start}}_{g,t}) + T^{\text{start}}_g \tag{7}$$

$$u_{w,t} \le u_{b_w,t} \tag{8}$$

$$u_{l,t} \le u_{n(m),t} \tag{9}$$

$$u_{l,t+1} \le (u_{n,t} + u_{m,t}) \tag{10}$$

*d) Generator Characteristics Constraints:* The output of a conventional generator $(P_{g,t}, Q_{g,t})$ should be bounded by its real and reactive power capacity. Similarly, the output of a wind farm $P_{w,t}$ should be capped at its forecasted value $\bar{P}_{w,t}$. This requirement is expressed in the following three constraints:

$$P^{\min}_g u^{\text{on}}_{g,t} \le P_{g,t} \le P^{\max}_g u^{\text{on}}_{g,t} \tag{11}$$

$$Q^{\min}_g u^{\text{on}}_{g,t} \le Q_{g,t} \le Q^{\max}_g u^{\text{on}}_{g,t} \tag{12}$$

$$P_{w,t} \le \bar{P}_{w,t} u_{w,t} \tag{13}$$

*e) Power Balance Constraints:* Real and reactive power generation and load have to be balanced at all times, as shown in constraints (14) and (15). Wind energy should be taken into account in balance constraints. We adopted the linearized model of AC power flow so as to attain the real and reactive power flow of lines. This approach introduces a piecewise linear approximation to AC power flow that considers voltage and reactive power [15]. In the literature, [16] adopts this approach to solve the deterministic optimization whose objective function is to minimize the interruption cost of unserved loads. Constraints (16) and (17) present the linearized active and reactive power flows. In (18), the cosine function is divided into $K$ equal sections and approximated by choosing appropriate values of $z_{nm,k}$ and $a_{nm,k}$. Constraint (19) is checked in each restoration time and enforces the voltage at each bus to remain within the limits.

$$\sum_{g\in G}(P_{g,t} - P^{\text{start}}_{g,t}) + \sum_{w\in W} P_{w,t} - \sum_{d\in D} P_{d,t} = \sum_{nm\in L} P^{\text{flow}}_{nm,t} \tag{14}$$

$$\sum_{g\in G} Q_{g,t} + \sum_{w\in W} Q_{w,t} - \sum_{d\in D} Q_{d,t} = \sum_{nm\in L} Q^{\text{flow}}_{nm,t} \tag{15}$$

$$P^{\text{flow}}_{nm,t} = (2V_{n,t} - 1)g_{nm} - (V_{n,t} + V_{m,t} + y_{nm,t} - 2)g_{nm} - b_{nm}\theta_{nm,t},\ n \ne m \tag{16}$$

$$Q^{\text{flow}}_{nm,t} = -(2V_{n,t} - 1)(b_{nm} + b^c_{nm}) + (V_{n,t} + V_{m,t} + y_{nm,t} - 2)b_{nm} - g_{nm}\theta_{nm,t},\ n \ne m \tag{17}$$

$$y_{nm,t} = z_{nm,k}\theta_{nm,t} + a_{nm,k},\ k = 0...K-1 \tag{18}$$

$$V^{\min} \le V_{n,t} \le V^{\max} \tag{19}$$

This article has been accepted for publication in a future issue of this journal, but has not been fully edited. Content may change prior to final publication. Citation information: DOI 10.1109/TSG.2017.2729592, IEEE Transactions on Smart Grid



*f) Load Characteristics and Load Pickup Constraints:* Real and reactive loads can be restored only after energizing their respective buses, as shown in (20) and (21).

$$0 \le P_{d,t} \le P_d^{\max} u_{b_d,t} \tag{20}$$

$$0 \le Q_{d,t} \le Q_d^{\max} u_{b_d,t} \tag{21}$$

Caution should be taken when restoring loads. If too much load is picked up, a large frequency dip can occur that will cause system instability. This becomes even more severe when wind turbines participate in restoration without inertial responses. Research has been conducted to enhance wind turbine contribution to frequency regulation through adding a supplementary control loop and releasing the hidden inertia. For instance, [17] and [18] have proposed a novel control strategy for variable speed wind turbines to enable them to actively participate in primary frequency control. Also, authors in [19] have shown that the inertial control effect can be translated into the system inertia, by which the equivalent system inertia is improved.

The maximum load pickup capability of system is a function of system inertia, governor response ramp rate, governors' dead band, and minimum allowable frequency drop (nadir) [20]. In (22), the maximum load pickup value in each restoration time is restricted to $\Delta P_t^{\max}$, where $RR_g$ (MW/s) is the maximum governor ramping rate for unit $g$, and $F = \sqrt{\frac{4.S_{\text{base}}(f^0 - f^{\min} - f^{\text{db}})}{f^0}}$. Note that through activation of inertial control strategy, the wind turbine inertia will contribute to the overall system inertia ($H_t^{\text{eq}} = \sum_{g\in G} H_g u_{g,t}^{\text{on}} + \sum_{w\in W} H_w u_{w,t}$) so that the transient response of power system can be improved subsequent to a load pickup.

$$\Delta P_t^{\max} \le F \sqrt{H_t^{\text{eq}} \sum_{g\in G} RR_g u_{g,t}^{\text{on}}} \tag{22}$$

The load pickup constraint is then written by,

$$0 \le \sum_{d\in D} P_{d,t+1} - \sum_{d\in D} P_{d,t} \le \Delta P_t^{\max} \tag{23}$$

The static load model, referred as the ZIP model [21], has been considered in this paper. Constraint (24) represents the voltage-dependent model of the loads, where $\beta_z$, $\beta_I$, and $\beta_p$ are the constant impedance, constant current and constant power coefficients. The non-linear ZIP load model together with its linear equivalent is presented in (24) [16]. Where, $V_0$ is the rated voltage, $P_{d,t}^{\text{V}_0}$ represents active power demand at rated voltage.

$$\begin{aligned} P_{d,t} &\le (\beta_p + \beta_I \frac{V_{b,t}}{V_0} + \beta_z (\frac{V_{b,t}}{V_0})^2) P_{d,t}^{\text{V}_0} \\ &\approx (\beta_p - \beta_z + \frac{V_{b,t}}{V_0}(\beta_I + 2\beta_z)) P_{d,t}^{\text{V}_0} \end{aligned} \tag{24}$$

*g) Dynamic Reserve Constraints:* Dynamic reserve is acquired to ensure system stability. Specifically, when contingencies occur, system frequency needs to be maintained within an acceptable range. The dynamic reserve comes from three reserve resources, including traditional generators, wind generators, and under-frequency load shedding (UFLS). Note that the UFLS should be less than 50% of the total reserve, according to industry practice [22]. Let $R_t$ denotes system reserve at time $t$, dynamic reserve constraints are given by

$$R_t \le \sum_{d\in D_{\text{UFLS}}} R_{d,t} + \sum_{g\in G} R_{g,t} + \sum_{w\in W} R_{w,t} \tag{25}$$

$$\sum_{d\in D_{\text{UFLS}}} R_{d,t} \le 0.5 R_t \tag{26}$$

For each individual energy source, including wind farms and conventional generators, the dynamic reserve should be bounded by its available capacity. Constraints (27) and (28) show the available headroom provided by the conventional generators and wind farms. Constraint (29) relates the maximum available dynamic reserve to the governor's characteristics, where $\Delta P_g$ shows the load pickup capability of generator $g$ that can be calculated using (22).

$$R_{g,t} \le P_g^{\max} - P_{g,t} \tag{27}$$

$$R_{w,t} \le \bar{P}_w - P_{w,t} \tag{28}$$

$$R_{g,t} \le \Delta P_g \tag{29}$$

To combat the loss of the largest generation, we need to make sure that the real power from traditional generators and wind generators do not exceed the total dynamic reserve:

$$P_{g,t} \le R_t - R_{g,t} \tag{30}$$

$$P_{w,t} \le R_t - R_{w,t} \tag{31}$$

## IV. Stochastic Optimization for Wind Uncertainty

The wind power available to participate in restoration is highly dependent on forecasting accuracy. In the aforementioned formulation, the maximum available wind power $\overline{P}_w$ is forecasted which can never be perfect. To handle the uncertainty, the deterministic formulation is now extended to stochastic optimization with scenarios.

### A. Scenario Generation and Reduction

The forecasting errors are modeled with scenarios generated using Latin hypercube sampling (LHS). We generate a large number of scenarios to completely describe the stochastic nature of the wind power. These scenarios are generated using the forecasted data, mean and standard deviation of the forecast error at every restoration time. Wind power forecast error is described using normal distribution function with a mean of zero and a standard deviation of $\alpha\%$, where parameter $\alpha$ can be adjusted by system operator. LHS method can accurately recreate the input distribution through sampling in fewer iterations compared with the Monte Carlo method. In this way, the probability density function (PDF) curve is divided into $N$ non-overlapping equiprobable intervals within which random sampling is performed. It guarantees that there

This article has been accepted for publication in a future issue of this journal, but has not been fully edited. Content may change prior to final publication. Citation information: DOI 10.1109/TSG.2017.2729592, IEEE Transactions on Smart Grid



will be precisely 1 sample in each interval such that the entire PDF space including the tails will be covered.

Having a large number of scenarios renders a large-scale mathematical problem. To mitigate the computational burden resulted from the problem size, an efficient scenario reduction algorithm is applied to produce a set of representative scenarios combined with their associated probabilities. A fast forward reduction technique based on Kantorovich distance has been adopted [23]. The aim is to select a subset $S$ from the generated scenario set $\Omega$ in a way that the representative scenarios have the shortest distance to the remaining scenarios.

### B. Stochastic Optimization

With the generated scenarios, the objective function of the restoration problem with wind participation now becomes:

$$\max \sum_{t\in T}\sum_{g\in G}(P_g^{\max}-P_g^{\text{start}})u_{g,t}^{\text{on}}+\sum_{t\in T}\sum_{w\in W}\bar{P}_{w,t}u_{w,t} - \sum_{s\in S}\pi_s\sum_{t\in T}\sum_{d\in D}\alpha_d(P_d^{\max}-P_{d,s,t}) \tag{32}$$

In each scenario, the simulated wind power takes in the place of the forecasted wind power, introducing different load pickup sequences and values. The set of decision variables which are contingent upon the scenarios and times are those in $\Xi_{\text{second}} = [P_{g,s,t}, Q_{g,s,t}, P_{w,s,t}, Q_{w,s,t}, P_{l,s,t}^{\text{flow}}, Q_{l,s,t}^{\text{flow}}, P_{d,s,t}, Q_{d,s,t}, R_{s,t}, R_{g,s,t}, R_{d,s,t}, R_{w,s,t}, \Delta P_{s,t}^{\max}]$. These decision variables pertain to the constraints (11)-(31). Even with a limited number of scenarios, the resulting problem requires the use of decomposition techniques so as to attain computational tractability.

## V. Integer L-shaped Decomposition

### A. Two-Stage Decomposition

A two-stage decomposition is employed to solve this large-scale combinatorial problem. The first-stage problem determines the online times of all generators, as well as line and bus enegization times. These decisions are common to any wind scenarios. Master problem (33) contains function $\varphi(x,s)$ representing the objective function of subproblems, as expressed in (34). Subproblems incorporate all decisions related to the load pickup values and locations, real and reactive power of all generators, and dynamic reserves. The subproblems decisions must be taken relative to the realization of uncertain wind power output.

$$MP: \min\Big(-\sum_{t\in T}(\sum_{g\in G}(P_g^{\max}-P_g^{\text{start}})u_{g,t}-\sum_{w\in W}\bar{P}_{w,t}u_{w,t}) + \sum_{s\in S}\pi_s\varphi(x,s)\Big) \tag{33}$$
$$\text{subject to: (2)–(10)}$$

where,

$$SP_s:\ \varphi(x,s)=\min\Big(\sum_{t\in T}\sum_{d\in D}\alpha_d(P_d^{\max}-P_{d,s,t})\Big) \tag{34}$$
$$\text{subject to: (11)–(31)}$$

### B. The Integer L-Shaped Algorithm

The integer L-shaped algorithm is applied to solve the two-stage stochastic restoration problems (33) and (34). This algorithm was proposed by Laporte and Louveaux and applied to solve the stochastic integer program [24]. Also, it has been adopted to solve the two-stage adaptive restoration problem [25]. In this method, master problem is relaxed and solved using branch-and-cut algorithm. For any feasible integer solution found, the subproblem is solved for each scenario and a set of optimality cuts are generated. Then, in the second iteration, the master problem is re-solved with optimality cuts generated in the previous iteration to obtain a new feasible solution. This process iteratively continues until the convergence criterion is met. The master problem (33) can be rewritten in a compact form (35):

$$\min_{x\in\{0,1\}^n}\left\{c^Tx+Q(x)\right\}$$
$$\text{subject to: } (2)-(7) \tag{35}$$

where $x$ represents the first-stage decision variables which are in set $\Xi_{\text{first}} = [u_{g,t}^{\text{on}}, u_{g,t}^{\text{start}}, u_{n,t}, u_{l,t}, u_{w,t}]$. $Q(x) = \sum_{s\in S}\pi_s\varphi(x,s)$ is called recourse function. The integer L-shaped algorithm proposed is shown in Fig. 2. Initially, we set iteration count $v=0$ and the best known objective function $\overline{z}=\infty$ (global upper bound). From the search tree, a node is selected, If such a node does not exist, the algorithm is terminated and the best solution is found. Otherwise, set $v=v+1$, solve the relaxed master problem (36).

$$RMP:\ \min_{x\in[0,1]^n}\left\{c^Tx+\phi\right\}$$
$$\text{subject to: } (2)-(7) \tag{36}$$

where $\phi \geq LB$, $LB$ is the global lower bound of the second-stage objective function, and $z$ is the objective function of RMP. If the current problem has no feasible solution or $z\geq\overline{z}$, fathom the current node and go to back to the search tree. If the current solution is not integer, create two new branches on fractional variables and append them to the list of pendent nodes. If the current solution is integer, solve the sub problems for each scenario, let $z^v=c^Tx^v+Q(x^v)$ and update the best solution $\overline{z}=min\{\overline{z},z^v\}$. If $\phi^v<Q(x^v)$, add the optimality cut (37), otherwise fathom the current node and choose another node from the search tree.

Let $x^v$ be the first-stage solution in iteration $v$, knowing that one can find its corresponding second-stage optimal solution $Q(x^v)$. The index set $I^v:=\{i:x_i^v=1\}$ represents the set of $v^{th}$ feasible solution and $|I(x^v)|$ showing the number of current first-stage decision variable with positive value. The general form of integer L-shape algorithm optimality cut for each wind scenario can be expressed as (37). The quantity

This article has been accepted for publication in a future issue of this journal, but has not been fully edited. Content may change prior to final publication. Citation information: DOI 10.1109/TSG.2017.2729592, IEEE Transactions on Smart Grid



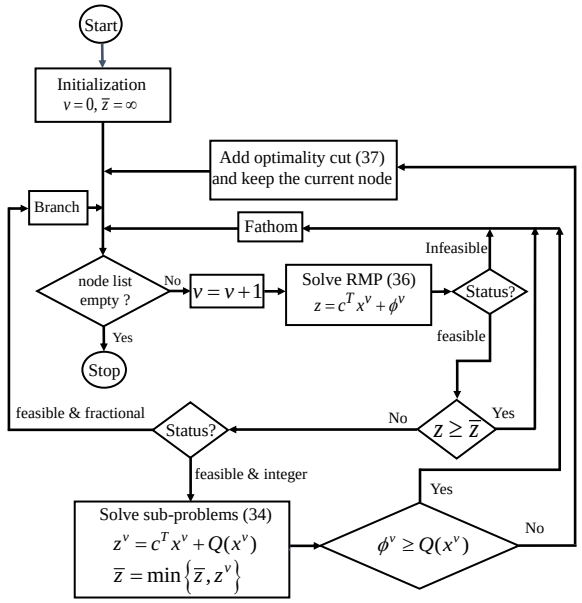


Fig. 2. Flowchart of integer L-shaped algorithm.

$\sum_{i\in I^v} x_i - \sum_{i\notin I^v} x_i$ takes the value of $|I(x^v)|$ when $x$ is the $v^{th}$ feasible solution. In such a case, the value of right-hand side of (37) becomes equal to $Q(x^v)$. Otherwise, if $\sum_{i\in I^v} x_i - \sum_{i\notin I^v} x_i$ is less than or equal to the $|I(x^v)|$, the right-hand side of the (37) is always less than or equal to global lower bound $LB$. Note that the integer L-shaped optimality cut is problem dependent and a large feasible space of $x$ with the complex second-stage MILP problem can increase the convergence time of the algorithm. Our method of only involving essential first-stage decision variables of $u^{\text{on}}_{g,t}$ and $u_{w,t}$ in the optimality cut (37) efficiently improves the convergence of algorithm.

$$\phi \geq (Q(x^v) - LB)\left\{\sum_{i\in I^v} x_i - \sum_{i\notin I^v} x_i - |I(x^v)| + 1\right\} + LB \tag{37}$$

## VI. Numerical Results

In this section, the impact of wind participation in power system restoration is thoroughly tested. We explore various factors, including wind generator location, penetration, fluctuation, inertia control capability, and uncertainty. The stochastic optimization is also compared with the deterministic and worst-case formulations to show the improvement in the total served energy.

Our test case is a modified IEEE 57-bus system as shown in Fig. 3. The total amount of de-energized load is 1250.5 MW. The characteristics of buses and transmission lines are taken from [26]. The characteristics of generators is shown in Table I. Tables II and III indicate loads' data and parameters of static load model. Parameters $f^{\min}$, $f^{\text{db}}$, and $f^0$ are set to 59.6 Hz, 36 mHz, and 60 Hz respectively. G1 is the BSU and the rest of units are NBSUs. A wind farm is connected at bus 38 with total installed capacity of 200 MW and inertia of 4 $s$.

TABLE I
Generators characteristics.

| Gen. No. | Pmax (MW) | Qmin (MVar) | Qmax (MVar) | H (s) | $P_g^{\text{start}}$ (MW) | $RR_g$ (MW/s) |
|---|---|---|---|---|---|---|
| G1 | 220 | -100.0 | 120.0 | 6 | 0.0 | 4.2 |
| G2 | 240 | -50.0 | 100.0 | 5.4 | 6.0 | 0.8 |
| G3 | 140 | -50.0 | 60.0 | 6.8 | 5.0 | 0.85 |
| G6 | 150 | -80.0 | 50.0 | 6.5 | 8.0 | 1.5 |
| G8 | 310 | -140.0 | 200.0 | 7.1 | 6.0 | 2.35 |
| G9 | 100 | -30.0 | 30.0 | 4.2 | 6.0 | 0.7 |
| G12 | 200 | -50.0 | 50.0 | 6.5 | 7.0 | 2.1 |

TABLE II
Loads' data and priorities.

| Load bus | $P_d^{\max}$ (MW) | Priority | Load bus | $P_d^{\max}$ (MW) | Priority |
|---|---|---|---|---|---|
| 1 | 55.0 | 0.9 | 29 | 17.0 | 0.9 |
| 2 | 3.0 | 1.0 | 30 | 3.6 | 1.0 |
| 3 | 41.0 | 1.0 | 31 | 5.8 | 1.0 |
| 5 | 13.0 | 1.0 | 32 | 1.6 | 0.8 |
| 6 | 75.0 | 0.8 | 33 | 3.8 | 1.0 |
| 8 | 150.0 | 1.0 | 35 | 6.0 | 0.8 |
| 9 | 121.0 | 1.0 | 38 | 14.0 | 0.9 |
| 10 | 5.0 | 0.8 | 41 | 6.3 | 1.0 |
| 12 | 377.0 | 0.9 | 42 | 7.1 | 1.0 |
| 13 | 18.0 | 0.8 | 43 | 2.0 | 1.0 |
| 14 | 10.5 | 0.8 | 44 | 12.0 | 1.0 |
| 15 | 22.0 | 1.0 | 47 | 29.7 | 0.8 |
| 16 | 43.0 | 0.8 | 49 | 18.0 | 1.0 |
| 17 | 42.0 | 0.9 | 50 | 21.0 | 1.0 |
| 18 | 27.2 | 1.0 | 51 | 18.0 | 1.0 |
| 19 | 3.0 | 0.9 | 52 | 4.9 | 1.0 |
| 20 | 2.3 | 1.0 | 53 | 20.0 | 1.0 |
| 23 | 6.3 | 1.0 | 54 | 4.1 | 0.8 |
| 25 | 6.3 | 1.0 | 55 | 6.8 | 1.0 |
| 27 | 9.3 | 1.0 | 56 | 7.6 | 1.0 |
| 28 | 4.6 | 1.0 | 57 | 6.7 | 0.8 |

TABLE III
Parameters of static load model.

| Load buses with ZIP loads | $\beta_p$ (%) | $\beta_I$ (%) | $\beta_z$ (%) |
|---|---|---|---|
| 1, 5, 10, 31, 49, 53, 57 | 7.0 | 78.0 | 15.0 |
| 2, 3, 16, 17, 19, 29, 44 | 6.0 | 63.0 | 31.0 |
| 6, 8, 14, 38, 41, 51, 55 | 5.0 | 84.0 | 11.0 |
| 9, 33, 35, 42, 52, 54, 56 | 2.0 | 84.0 | 14.0 |
| 12, 13, 15, 18, 20, 23, 32 | 2.0 | 89.0 | 9.0 |
| 25, 27, 28, 30, 43, 47, 50 | 1.0 | 63.0 | 36.0 |

In all cases the base power is assumed to be 100 MW and each restoration time step is 10 minutes (1 p.u.) which is required for preparation and frequency stabilization. Also, wind farm is operated at unity power factor. Loads are assumed to be fully dispatchable and load restoration actions are taken at the beginning of each restoration time step. The integer L-shape algorithm is codded in C++ using CALLBACK function of IBM ILOG CPLEX 12.6. All simulations were executed on a PC with Intel CoreTM i5 CPU @3.30 GHz and 8 GB RAM.

This article has been accepted for publication in a future issue of this journal, but has not been fully edited. Content may change prior to final publication. Citation information: DOI 10.1109/TSG.2017.2729592, IEEE Transactions on Smart Grid



TABLE IV
GENERATORS' OPTIMAL ON TIME AND TYPES.

| Gen. No. | Time (p.u.) | Type unit | Gen. No. | Time (p.u.) | Type unit |
|---|---|---|---|---|---|
| G1 | 2 | Gas turbine | G8 | 10 | Gas turbine |
| G2 | 7 | Steam turbine | G9 | 9 | Steam turbine |
| G3 | 8 | Steam turbine | G12 | 8 | Gas turbine |
| G6 | 10 | Gas turbine | | | |

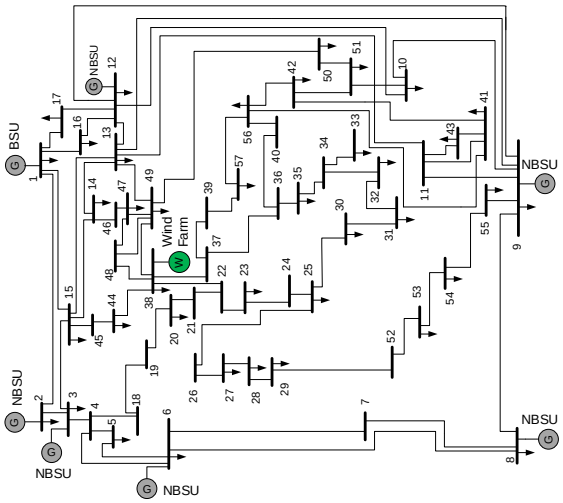


Fig. 3. Modified IEEE 57-bus test case.

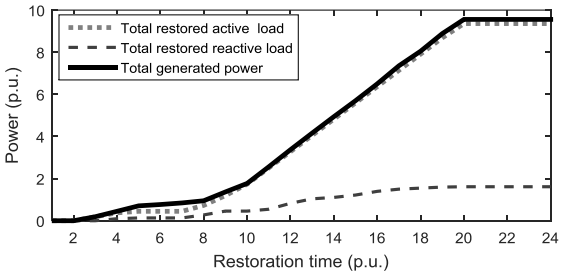


Fig. 4. Total generated power and real and reactive load pickup in the base case.

## A. Harnessing Wind Power for Restoration

To investigate the wind impact, a base case benchmark is first established where the wind farm is excluded from the restoration process. Table IV indicates the on times of conventional generating units in the base case. The BSU G1 becomes online at $t = 2$ restoration time. The first load bus is energized at $t = 3$ when the load pickup process can be started. The first NBSU becomes online after $t = 7$ restoration time. Fig. 4 depicts the total generation and load pickup curves of the base case, where the total restored load is 936 MW and the total energy served is 1.66 GWh. Note that without wind participation, the system cannot be completely restored. Now assume that the wind farm is allowed to fully participate in the restoration process. The wind impact is investigated from the following aspects: location, penetration, fluctuation, and inertia capability. Finally, replacement of conventional generation units by wind farm is also studied.

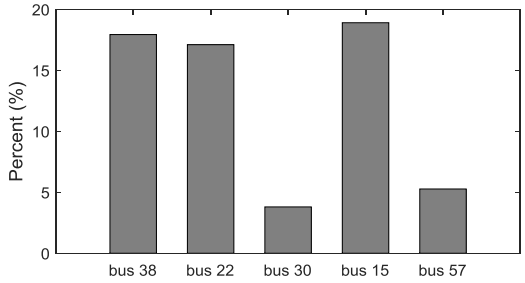


Fig. 5. Total energy served at different wind farm locations respect to the base case.

*a) Impact of wind location:* Besides the wind farm output power profile, its location has a direct impact on the restoration process. Fig. 5 compares the total energy served with respect to different wind farm locations and under the same output power profiles. It shows the percentage of increase in the total energy served compared with the base case. For instance, the 200 MW wind farm installed at bus 15 will improve the total energy served by 1.18% and 18.9% versus that installed at bus 38 and the base case, respectively. However, in practice, wind profile changes from location to location and using the proposed tool enable system operators to measure the contributions of wind farms installed at a variety of geographical locations.

*b) Impact of wind penetration:* The wind farm installed at bus 38 has capacity of 200 MW, representing 16% penetration. We then increase the wind farm capacity to 400 MW, representing 32% penetration. The restoration results are shown in Figs. 6 and 7. In the low penetration case, the total energy served is 1.99 GWh, while this number is improved to 2.15 GWh in the high penetration case. Comparing two cases, one can see that although the higher wind penetration leads to better restoration performance, the total energy served has not improved proportionally. In contrast, more wind energy spillage has been observed in the second case. This implies that only a certain amount of wind energy can contribute to the restoration, owing to the limited load pickup capability at early stages and dynamic reserve restriction at the final stages.

*c) Impact of Wind Fluctuation:* Wind fluctuation levels can differ from time to time. Highly fluctuated wind power could result in severe ramping events. In Fig. 8 (a), one can observe a large fall and rise in the wind farm power where the minimum value reached to 50 MW at $t = 10$. The total energy served is 1.93 GWh, a slightly decrease from Fig. 6. If this ramping event occurs at $t = 15$ as shown in Fig. 8 (b), the wind generation curve will be different than that at $t = 10$. More importantly, the total restored energy is now decreased to 1.86 GWh, and the load pickup curve gets close to the base case curve at $t = 16$ and $t = 17$. For $t \geq 20$ in both cases, it can be seen that the load restoration curves with wind exceed the base case curve meaning that the majority of loads become served with the wind power contribution. The results indicate that not only the fluctuation level matters, but also the fluctuation times play a critical role in deploying wind power for restoration.

This article has been accepted for publication in a future issue of this journal, but has not been fully edited. Content may change prior to final publication. Citation information: DOI 10.1109/TSG.2017.2729592, IEEE Transactions on Smart Grid



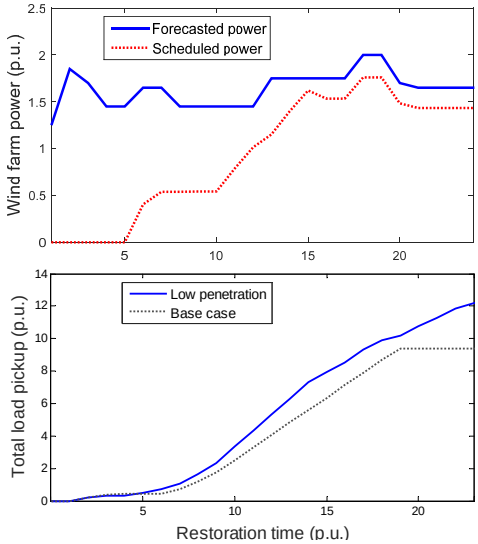


Fig. 6. Wind power and load pickup with the 200MW wind farm at bus 38.

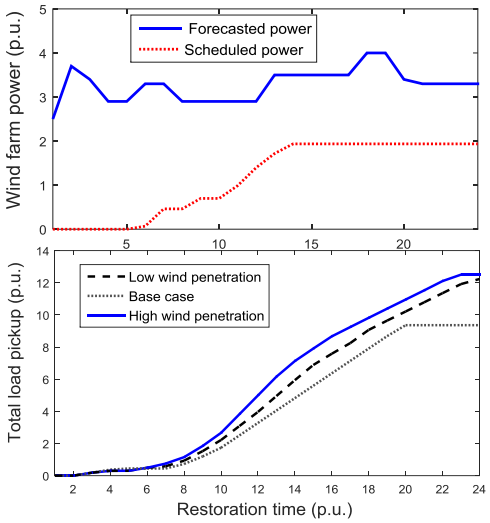


Fig. 7. Wind power and load pickup with the 400MW wind farm at bus 38.

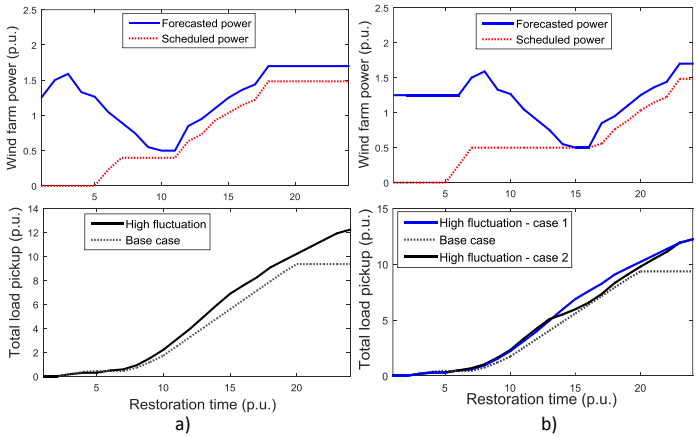


Fig. 8. Wind power with fluctuations at different restoration times.

*d) Impact of Wind Inertial Control Capability:* An active inertia emulation control of wind generators can contribute to system frequency, load pickup, and dynamic reserve. Without wind generators' inertial control capability, the total restored energy is 1.74 GWh. This number is improved to 1.99 GWh with active inertial control. From Fig. 9, one can see that the wind farm can help restoration even without the inertial control capability, but the contribution is limited until the end of load pickup. When the inertial control is activated, the wind farm can freely participate and start contributing from the very early stage of restoration process. The contributions include the cranking power for NBSUs at the initial stages, and the support of NBSUs in load pickup and dynamic reserve at the final stages.

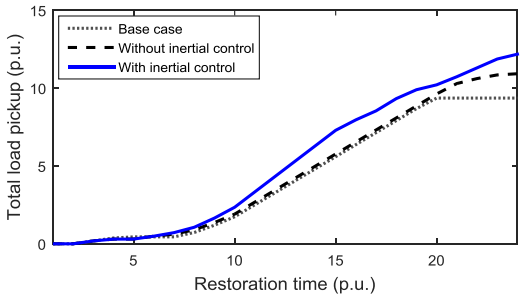


Fig. 9. Total load pickup with and without inertial control.

*e) Impact of Replacing Conventional Generation Units by the Wind Farm:* Replacement of fossil fuel units by a large-scale wind farm is very likely to occur in smart grids. To study this case, we assumed that generation unit G12 is replaced by the same size of wind farm with activated inertial control. The wind farm output power profile is similar to one presented in Fig. 6. Comparison of the load pickup curve of this case with the base case is depicted in Fig. 10. The total restored energy becomes 1.54 GWh, showing a reduction of 105 MWh with respect to the base case. At initial stages (i.e. $4 \leq t \leq 7$), one can observe an improvement in the restoration curve with the wind farm. This comes from the fact that wind turbines are fast-starting units without demanding cranking power from the BSU. Thus, as opposed to the conventional generation units, their capacity will immediately be available for restoration purpose. Also, BSU does not provide their cranking powers, but it devotes its full capacity for restoring loads. At final stages, wind profile and wind farm's load pickup capability are the dominant factors that specify the total restored energy. We observe a slight reduction in load restoration curve compared to the base case. This reduction would become more significant with the higher fluctuations of wind farm output power, particularly at final stages.

## *B. Stochastic Optimization Performance*

Assuming the wind energy forecasts are perfect, one can obtain the "expected value of perfect information" (EVPI), which serves as an upper bound for the total served energy in the restoration process. However, this solution never exists in reality. The formulated stochastic optimization is able to capture the uncertainty from wind energy during the restoration process. It is a common practice in the literature to assume a normally distributed wind power prediction error whose

This article has been accepted for publication in a future issue of this journal, but has not been fully edited. Content may change prior to final publication. Citation information: DOI 10.1109/TSG.2017.2729592, IEEE Transactions on Smart Grid



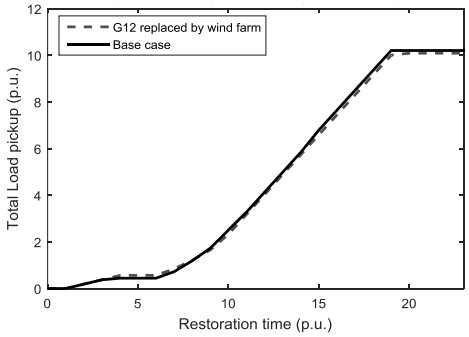


Fig. 10. Total load pickup when G12 is replaced by the 200MW wind farm.

standard deviation increases with the prediction horizon [27], [28]. For restoration period, we assumed that the standard deviation of this error is $\alpha = 10\%$. For the testing purpose, 5000 scenarios are generated using the LHS sampling method and then reduced to 10 representative scenarios with assigned probability, as shown in Fig. 11. The "value of stochastic solution" (VSS) can be obtained for the expected energy served under all scenarios. In contrast, another way is to take the expected wind energy from all scenarios and solve the deterministic problem (1). The obtained objective function is then called "expected value solution" (EVS). Finally, we run the optimization problem for the worst-case condition in which the worst possible scenario of wind power fluctuations are taken into consideration. In other words, the stochastic deviations of wind power are replaced by the constant deviations for entire restoration period.

Note that perfect information always yields the best result. Fig. 12 gives the percentage of decrease from EVPI (in terms of total energy served) for VSS, EVS, and worst-case. We conducted simulations for two cases, with and without inertial control. In both cases, one can see that the VSS outperforms EVS; it shows greater impact without having inertial control in operation. Also, the approach of considering the worst-case scenario provides a very conservative estimation result. This approach could become worse in cases where uncertain parameters have a large range of variability. However, when the uncertainties cannot be described by probability distribution functions, the worst-case scenario or robust optimization method [29] could be a viable solution to address this limitation.

*a) Multiple Wind Farms Distributed in Different Locations:* Now we consider a real case where four identical wind farms with maximum generation capacity of 50 MW are geographically distributed in four locations, buses 13, 29, 31, and 38, as wind farms 1-4. Wind farm forecasted power profiles are shown in Fig. 13. These four locations are chose strategically to represent four corner areas of the test system. The stochastic optimization is run to determine the optimal restoration planning solution. Fig. 14 shows the optimal dispatch solutions for different wind farms. It can be seen that wind farm 4, located at bus 38, is connected at $t = 6$, wind farms 2 and 3 are connected at $t = 12$, and wind farm 1 is the last one that is connected at $t = 14$.

Fig. 15 shows the total load pickup curve together with the

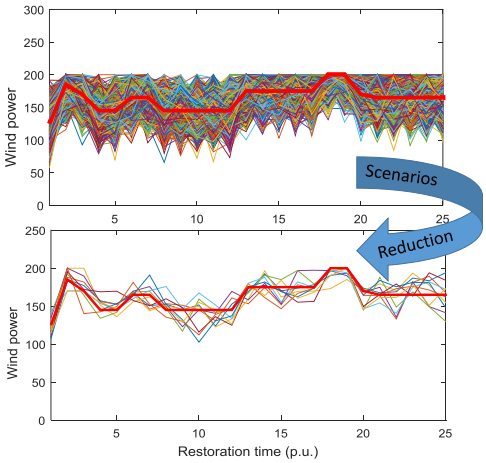


Fig. 11. 5000 scenarios are generated and reduced to 10 representative scenarios.

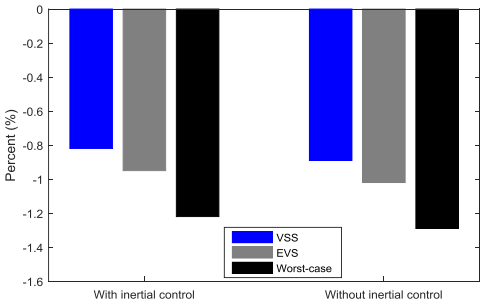


Fig. 12. Percentage of decrease from EVPI for VSS, EVS, and worst-case.

aggregated generation of wind farms at each restoration period. It can be seen that wind power is supplying the majority of the loads at $t = 6$ and $t = 7$ restoration times. However, during the restoration times $t = 7$ to $t = 12$, the share of wind farms remains constant. From this time forth, wind farms 2 and 3 are contributing to the restoration which increase the aggregated generation of wind farms. Ultimately, at the end of the restoration period, certain amount of wind power can be harnessed to assist the restoration process. It is worth noting that with considering wind uncertainty, 0.59% of total energy served comes from wind farm 4, 0.34% from wind farm 3, 0.19% from wind farm 2, and 0.32% from wind farm 1.

Fig. 16 shows the percentage of wind energy that are utilized or wasted in each wind farm. It can be seen that wind farm 4 has the highest level of wind energy utilization. Whereas, wind farm 2 has the highest level of energy spillage, although wind farm 1 is the last one became connected to the grid. The higher energy spillage in wind farm 2 is related to the ramp-down event taking place during the restoration period.

In Fig. 17, the impact of increasing the standard deviation of wind prediction error on the restoration process has been studied. This curve helps us to further elaborate the effect of wind uncertainty on each restoration step. The bar graphs are the absolute values of changes in total served load with respect to the perfect prediction case shown in percent. As expected, when the standard deviation of prediction error ($\alpha$) increases, total served load will decrease. However, it does

This article has been accepted for publication in a future issue of this journal, but has not been fully edited. Content may change prior to final publication. Citation information: DOI 10.1109/TSG.2017.2729592, IEEE Transactions on Smart Grid



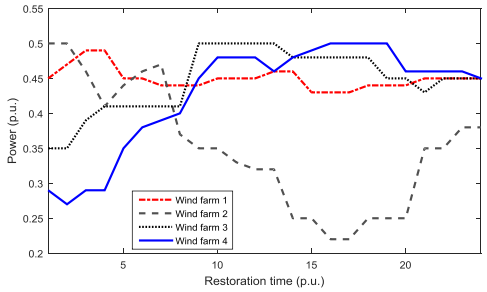


Fig. 13. Wind farms forecasted power in four locations.

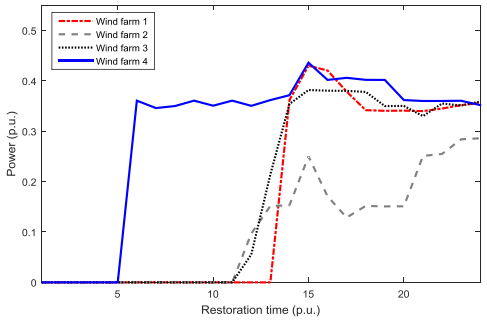


Fig. 14. Wind farms scheduled power obtained from stochastic optimization.

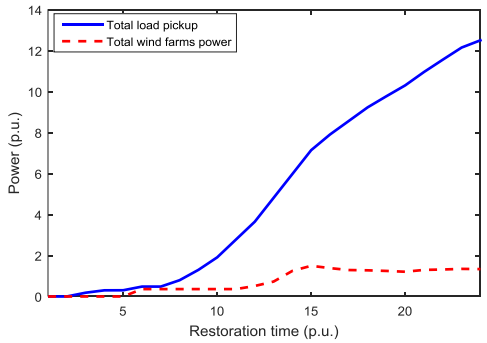


Fig. 15. Total load pickup curve obtained from the stochastic optimization together with the aggregated generation of wind farms.

not show an identical influence on different restoration steps. In fact, there is no influence at $t < 6$ p.u., since wind farms are not contributing to the restoration process in these times. However, we observe a significant impact at the initial stages of restoration compared to the other stages. This signifies the importance of having accurate forecasting tool in the initial stages so as to harness more wind energy, serve more loads, and reduce the restoration time.

*b) Computational Performance:* CPLEX stops processing and declares integer optimality when it finds an integer solution and all parts of the search space have been processed. In the planning phase of the restoration, when this problem is run, the computation time is a crucial factor. Thus, in this paper we set the tolerance to 0.005 which indicates to CPLEX to stop when an integer feasible solution proved to be within 0.5% of optimality. For IEEE 57-bus system, the total number of integer variables in the first-stage is 6,050 and the total number of variables in the second-stage is 28,525 per scenario.

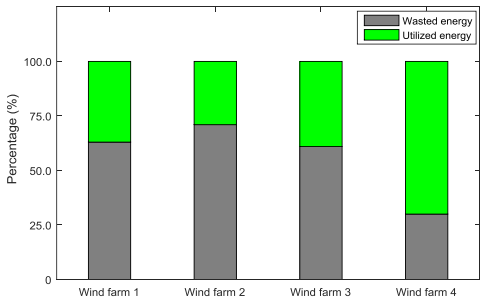


Fig. 16. The percentage of wind energy utilization and spillage for different wind farms.

The convergence time for one scenario without adopting the proposed decomposition approach is 1094.4 s. However, after adopting the decomposition method, the solution time is decreased to 86.8 s. In the case of 10 scenarios, we enabled the multiple thread feature of CPLEX and the convergence time becomes 774.8 s. A tighter MIP tolerance (e.g. 0.001) may be advantageous to avoid any chance of missing the best possible solution. But it drastically increases the computation time from 774.8 s to 1,932 s.

### C. Dynamic Response Validation Tool

In order to verify the results of the planning tool proposed in this paper, a dynamic validation tool has been designed and implemented as shown in Fig. 18. The output of optimization problem is first written in Microsoft Excel file, then read by Python scripts. Python is a high level programming language which can be used to run multiple Power System Simulation for Engineer (PSS/E) cases for a given power network. Finally, simulation results will be exported to an Excel file. Such a tool enables us to examine the dynamic behavior of system at each restoration step. In this simulation, we adopted the IEEE type DC1A excitation system model, GENROU is selected to represent the round rotor generator, GAST and IEEEG1 represent the governor model of gas and steam turbines, respectively [30].

Considering the case where 200 MW wind farm is installed at bus 38, a case study corresponding to the output results of the optimization problem at $t = 6$ p.u. is generated by using Python scripts. Note that the restoration curve of this case is shown in Fig. 6. The PSS/E simulation is run and the frequency trace as well as voltage profiles of buses are analyzed. Fig. 19 compares the frequency and real power of a wind farm with/without providing primary frequency response after picking up 23 MW of load at $t = 10$ $s$. It should be noted that, at this restoration step, only the BSU and wind farm are online and supplying the energized loads. Obviously with emulating inertia and offering primary frequency regulation, the frequency dip is reduced and hence more load can be restored. It can be seen that when wind farm does not participate in primary frequency response, the minimum frequency (nadir) exceeds its minimum limit (59.6 Hz). In such a case, it is highly likely that under-frequency load shedding relays are activated that will cause power outages during the restoration period.

This article has been accepted for publication in a future issue of this journal, but has not been fully edited. Content may change prior to final publication. Citation information: DOI 10.1109/TSG.2017.2729592, IEEE Transactions on Smart Grid



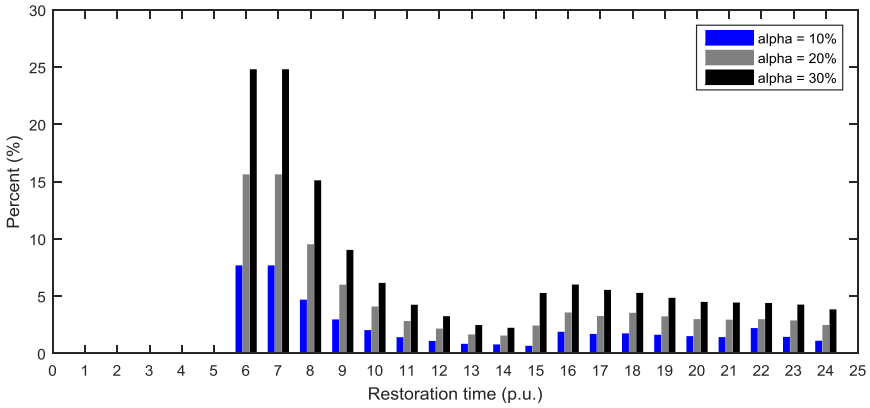


Fig. 17. The absolute values of changes in total served load with respect to the perfect forecast case when standard deviation of forecasting error increases ($\alpha = 10\%, 20\%$, and $30\%$).

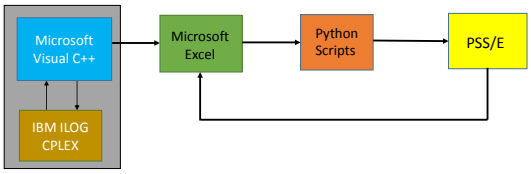


Fig. 18. The proposed dynamic response validation tool.

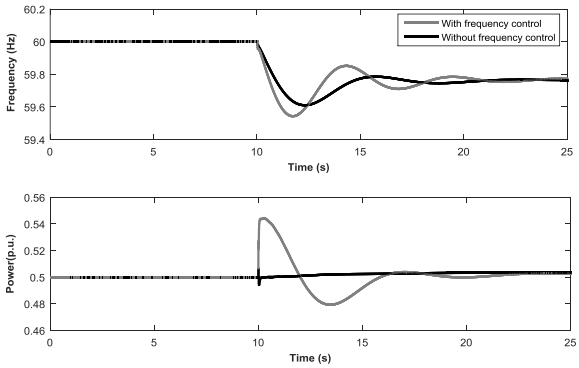


Fig. 19. Response of wind farm to 23 MW of load pickup with/without supplementary control loop activation.

Additionally, the voltage profiles of all energized buses should be examined to verify that their magnitudes do not exceed the minimum and maximum limits after a transient event. Fig. 20 depicts the voltage profiles of some buses after a load pickup action. One can observe a voltage dip at the instant of load pickup ($t = 10\ s$) due to the transient behavior of loads. Bus voltages are safely recovered after excitation system comes into effect so as to compensate voltage oscillations during transient period.

## VII. Conclusions

In this paper, we developed an offline restoration planning tool that can be used by TSOs to securely harness wind energy sources during the restoration process. The proposed decomposition approach efficiently mitigate the computational burden. This tool is able to help system operators get insight into where, when, and how much wind should be utilized at each restoration time. In particular, when there are several wind generators distributed all over the power grid with different penetration levels, output power forecasts, and ancillary services, this tool can determine the optimal wind dispatch decisions to minimize the restoration time. Finally, by incorporating a detailed dynamic simulation tool into the proposed planning tool, the results of stochastic optimization problem have been tested and verified.

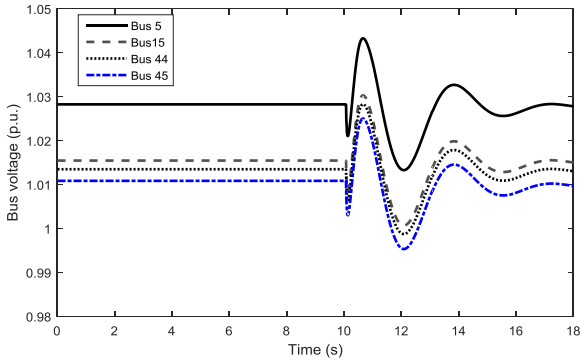


Fig. 20. Voltage profiles of buses 5, 15, 44, 45 after a load pickup.

The directions for future research that stem from this work are summarized as follows. 1) Development of the real-time optimization tool for restoration problem by adopting the efficient optimization methods such as sliding window or distributed optimization and control approaches. Computational burden and communication latency are two major challenges that should be taken into consideration. 2) Study the impacts of utilizing energy storages and performing an efficient coordination of storage and renewable during the restoration period. Such a coordination can further reduce our reliance on fossil fuel units, improve the renewable energy utilization, and shorten restoration time.

## References

[1] Wind Vision: A new era for wind power in the United States, U.S. Department of Energy, 2015, [Online]. Available: https://www.energy.gov/sites/prod/files/2015/03/f20/wv_full_report.pdf.

[2] A. Tuohy, P. Meibom, E. Denny, and M. OMalley, "Unit commitment for systems with significant wind penetration," *IEEE Trans. Power Syst.*, vol. 24, no. 2, pp. 592–601, May 2009.

[3] J. Hetzer, C. Yu, and K. Bhattarai, "An economic dispatch model incorporating wind power," *IEEE Trans. Energy Convers.*, vol. 23, no. 2, pp. 603–611, Jun. 2008.

[4] M. Amin and A. Giacomoni, "Smart grid, safe grid," *IEEE Power Energy Mag.*, vol. 10, no. 1, pp. 33–40, Jan/Feb. 2012.

[5] Black system south Australia, Mar. 2017, [Online]. Available: http://www.aemo.com.au/-/media/Files/Electricity/NEM/Market_Notices_and_Events/Power_System_Incident_Reports/2017/Integrated-Final-Report-SA-Black-System-28-September-2016.pdf.

[6] Ontario power system restoration Plan, 2016, [Online]. Available: http://www.ieso.ca/documents/systemOps/so_OntPowerSysRestorePlan.pdf

[7] H. Zhu and Y. Liu, "Aspects of power system restoration considering wind farms," In *Proc. Int. Conf. on Sustainable Power Generation and Supply* Sept. 2012, pp. 1–5.

[8] M. Aktarujjaman, M.A. Kashem, M. Negnevitsky, and G. Ledwich, "Black start with DFIG based distributed generation after major emergencies," In *Proc. Int. Conf. on Power Electronics, Drives and Energy Systems*, Dec. 2006, pp. 1–6.

[9] L. Seca, H. Costa, C. L. Moreira, and J. A. Lopes, "An innovative strategy for power system restoration using utility scale wind parks," In *Proc. Bulk Power System Dynamics and Control-IX Optimization, Security and Control of the Emerging Power Grid*, Aug. 2013, pp. 1–8.

[10] A. M. El-Zonkoly, "Renewable energy sources for complete optimal power system black-start restoration," *IET Gener. Transm. Distrib.*, vol. 9, no. 6, pp. 531–539, Apr. 2015.

[11] Y. Hou, C.C. Liu, K. Sun, P. Zheng, S. Liu, and D. Mizumura, "Computation of milestones for decision support during system restoration," *IEEE Trans. Power Syst.*, vol. 26, no. 3, pp. 1399–1409, Jun. 2011.

[12] M. M. Adibi and L. H. Fink, "Special considerations in power system restoration," *IEEE Trans. Power Syst.*, vol. 7, no. 4, pp. 1419–1427, Nov. 1992.

[13] MISO power system restoration Plan, 2016, [Online]. Available: https://www.misoenergy.org/Library/Repository/Procedure/RTO-PSR-001 MISO Power System Restoration Plan Manual Volume I Version9.1.pdf

[14] W. Sun, C. C. Liu, and L. Zhang, "Optimal generator start-up strategy for bulk power system restoration," *IEEE Trans. Power Syst.*, vol. 26, no. 3, pp. 1357–1366, Jun. 2011.

[15] P. A. Trodden, W. A. Bukhsh, A. Grothey, and K. I. M. McKinnon, "Optimization-based islanding of power networks using piecewise linear AC power flow," *IEEE Trans. Power Syst.*, vol. 29, no. 3, pp. 1212–1220, May 2014.

[16] A. Gholami and F. Aminifar, "A hierarchical response-based approach to the load restoration problem," *IEEE Trans. Smart Grid*, to be published.

[17] A. Zertek, G. Verbic, and M. Pantos, "A novel strategy for variable-speed wind turbines participation in primary frequency control," *IEEE Trans. Sustain. Energy*, vol. 3, no. 4, pp. 791–799, Oct. 2012.

[18] K. V. Vidyanandan and N. Senroy, "Primary frequency regulation by deloaded wind turbines using variable droop," *IEEE Trans. Power Syst.*, vol. 28, no. 2, pp. 837–846, May 2013.

[19] J. M. Mauricio, A. Marano, A. G. Exposito, and J. L. M. Ramos, "Frequency regulation contribution through variable-speed wind energy conversion systems," *IEEE Trans. Power Syst.*, vol. 24, no. 1, pp. 173–180, Feb. 2009.

[20] H. Chavez, R. Baldick, and S. Sharma, "Governor rate-constrained OPF for primary frequency control adequacy," *IEEE Trans. Power Syst.*, vol. 29, no. 3, pp. 1473–1480, May 2014.

[21] A. Bokhari, A. Alkan, A. Sharma, R. Dogan, M. Diaz-Aguilo, F. de Len, D. Czarkowski, Z. Zabar, A. Noel, and R. Uosef, "Experimental determination of the ZIP coefficients for modern residential, commercial, and industrial loads," *IEEE Trans. Power Del.*, vol. 29, no. 3, pp. 1372–1381, June 2014.

[22] PJM Manual 36: System Restoration. [Online]. Available: https://www.pjm.com/documents/manuals.aspx, 2013.

[23] J. Dupacov, N. Grwe-Kuska, and W. Rmisch, "Scenario reduction in stochastic programming: An approach using probability metrics," *Math. Program. Series A*, vol. 3, pp. 493–511, 2003.

[24] G. Laporte and F.V. Louveaux, "The integer L-shaped method for stochastic integer programs with complete recourse," *Oper. Res. Lett.*, vol. 13, pp. 133–142, Apr. 1993.

[25] A. Golshani, W. Sun, Q. Zhou, Q. P. Zheng, and J. Tong, "Two-stage adaptive restoration decision support system for a self-healing power grid," *IEEE Trans. Ind. Informat.*, to be published.

[26] IEEE 57-bus data. [Online]. Available: http://icseg.iti.illinois.edu/ieee-57-bus-system.

[27] F. Bouffard and F. D. Galiana, "Stochastic security for operations planning with significant wind power generation," *IEEE Trans. Power Syst.*, vol. 23, no. 2, pp. 306–316, May 2008.

[28] R. Doherty and M. OMalley, "A new approach to quantify reserve demand in systems with significant installed wind capacity," *IEEE Trans. Power Syst.*, vol. 20, no. 2, pp. 587–595, May 2005.

[29] R. Jiang, J. Wang, and Y. Guan, "Robust unit commitment with wind power and pumped storage hydro," *IEEE Trans. Power Syst.*, vol. 27, no. 2, pp. 800–810, May 2012.

[30] Siemens Power Technologies International, PSS/E 34.0 Model Library. New York, NY, USA: Siemens Industry Inc., 2013.